

Supplementary Information

New fluorescence light-up quinoxalines differentiate between parallel and nonparallel G-quadruplex topologies using different excitation/emission channels

Ming-Hao Hu^{*a}, Xiao Chen^b

^a School of Pharmaceutical Sciences, Shenzhen University Health Science Center, Shenzhen 518060, China

^b Zhuhai Institute for Food and Drug Control, Zhuhai 519000, China

Table of Contents:

Experimental Section	S2
Scheme S1. Synthesis of the compounds	S4
Table S1. DNA sequences used in the present study	S6
Figure S1. Concentration-dependent absorption spectra of the compounds in Tris-HCl buffer	S6
Figure S2. Absorption spectra of the quinoxaline derivatives at 5 μ M in Tris-HCl buffer	S7
Figure S3. Fluorescence spectra of the quinoxaline derivatives at 1 μ M in Tris-HCl buffer	S7
Figure S4. Fluorescence spectra of the quinoxaline derivatives with types of nucleic acids	S8
Figure S5. Absorption spectra of QC-1 upon gradual addition of types of nucleic acids	S8
Figure S6. Fluorescence intensities of QC-1 -pu22 complex with addition of competitive ds-DNA	S9
Figure S7. Fluorescence spectra of 1 μ M QC-1 with the stepwise addition of G4s	S9
Figure S8. CD spectra of parallel and nonparallel G4s with or without QC-1	S9
Figure S9. Job plot analysis for the binding stoichiometry of QC-1 to parallel G4 pu22	S10
Figure S10. CD spectra of QC-1 with or without parallel G4 pu22	S10
Figure S11. Imino proton regions of the ¹ H-NMR spectra of nonparallelG4 tel24 with QC-1	S11
Figure S12. Job plot analysis for the binding stoichiometry of QC-1 to nonparallel G4 tel22	S11
Figure S13. CD melting curves for G4s in the absence and presence of QC-1	S12
Figure S14. Aromatic regions of the ¹ H-NMR spectra of QC-1 without and with G4	S12
Figure S15–26. ¹ H NMR and ¹³ C NMR spectra of the final compounds	S13
References	S19

Experimental Section

Oligonucleotides and Compounds

All the oligonucleotides were dissolved in Tris-HCl buffer (10 mM, pH 7.2). Their concentrations were determined using NanoDrop 1000 Spectrophotometer (Thermo Scientific, USA). To obtain G4s, oligonucleotides were annealed in Tris-HCl buffer containing KCl by heating at 95 °C for 5 min, followed by gradual cooling to room temperature. The structures were then determined by CD. Stock solutions of compounds (10 mM) were dissolved in DMSO and stored at -80 °C. Further dilutions of samples to working concentrations were made with Tris-HCl buffer immediately prior to use.

Absorption Studies

Absorption studies were performed on a UV-2450 spectrophotometer (Shimadzu, Japan) using 1 cm path length quartz cuvette. All oligonucleotides were firstly prepared through heating at 95 °C for 5 min followed by slow cooling to room temperature. For titration experiments, small aliquots of a stock oligonucleotide solution were added into the solution containing **QC-1** at a concentration of 5 μ M in Tris-HCl buffer (10 mM, pH 7.2) with 100 mM KCl. After each addition, the reaction was stirred and allowed to equilibrate and its absorbance measurement was taken.

Fluorescence Studies

Fluorescence studies were performed on an F-4600 fluorescence spectrophotometer (Hitachi, Japan). A quartz cuvette with 2 mm \times 10 mm path length was used for the spectra recorded at 5 nm excitation and emission slit widths. All oligonucleotides were firstly prepared through heating at 95 °C for 5 min followed by slow cooling to room temperature. For titration experiments, small aliquots of a stock solution of the DNA sample were added into the compound solution at a concentration of 1 μ M in Tris-HCl buffer (10 mM, pH 7.2) with 100 mM KCl. After each addition, the reaction was stirred and allowed to equilibrate and fluorescence measurement was taken at $\lambda_{\text{ex}} = 450$ nm or 550 nm. For competitive fluorescence titrations, duplex DNA hairpin was gradually added into the complex solution containing **QC-1** (1 μ M) and pu22 (2 μ M). The final concentration of hairpin was varied from 0 to 25 μ M. The fluorescence measurement was taken at $\lambda_{\text{ex}} = 450$ nm.

NMR Studies

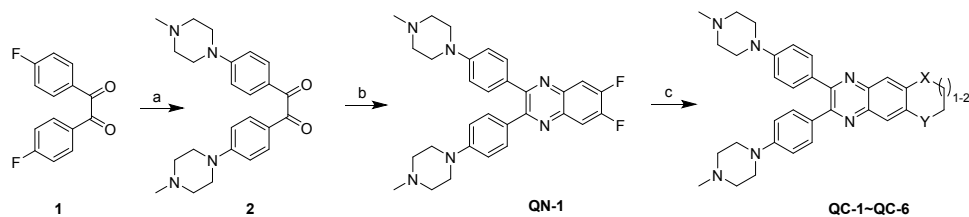
G4 samples for 1D ^1H -NMR were prepared in 25 mM potassium phosphate buffer (pH 7.2) containing 70 mM KCl and 10% D_2O . The final concentration of G4 DNA was 200 μM , titrated with increasing amounts of **QC-1**. Experiments were performed on a 600 MHz spectrometer (Bruker) at 25 $^\circ\text{C}$.

Circular Dichroism Studies

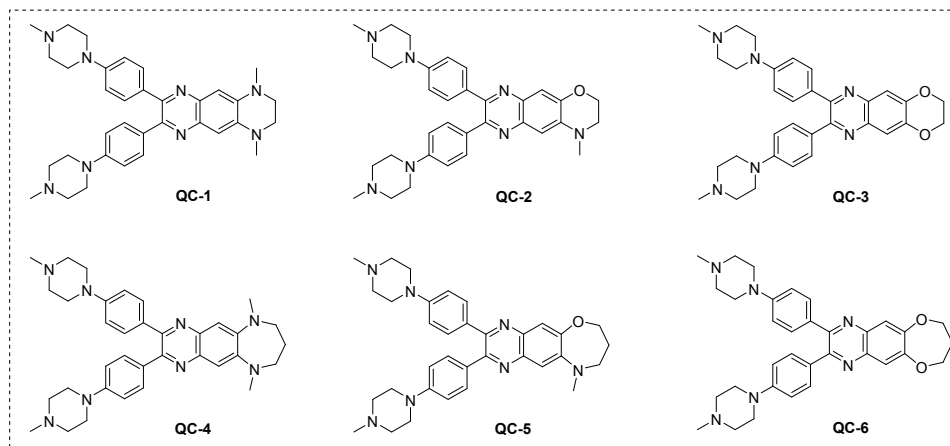
CD studies were performed on a Chirascan circular dichroism spectrophotometer (Applied Photophysics, UK). A quartz cuvette with a 10 mm path length was used for the recording of spectra with a 1 nm bandwidth, 1 nm step size and time of 0.5 s per point. Melting assays were conducted at a fixed G4 concentration (2 μM), either with or without **QC-1** (6 μM) in Tris-HCl buffer with KCl. The data were recorded at intervals of 5 $^\circ\text{C}$ over a range of 25–95 $^\circ\text{C}$ with a heating rate of 1 $^\circ\text{C}/\text{min}$. To observe the induced CD signals, the compound concentration was fixed at 30 μM , either with or without G4 samples (20 μM), and the spectra corresponding to the absorption region of **QC-1** were recorded.

2-Ap Experiments

Solutions containing 1 μM of 2-Ap-labelled G4s in 10 mM Tris-HCl buffer (pH 7.2, 100 mM KCl) were prepared. Each solution was heated at 95 $^\circ\text{C}$ for 5 min to remove any aggregates and then cooled slowly to 25 $^\circ\text{C}$. Afterwards, **QC-1** was gradually added to the 2-Ap-labeled G4 solution. The final concentration of **QC-1** was varied from 0 to 5 μM . After each addition of **QC-1**, the reaction was stirred and allowed to equilibrate, and the fluorescence measurement at 370 nm was taken when excited at 305 nm. In parallel, the same experiments were done using the non-labelled G4s for the sake of background subtraction.



Reagents and conditions: (a) N-methylpiperazine (5 equiv.), K_2CO_3 , DMSO, 90 °C, 5 h; (b) EtOH, CH_3COOH (cat.), reflux, 24 h; (c) K_2CO_3 , DMF, 100 °C, overnight.



Scheme S1. Synthesis of **QC-1–QC6**

Synthesis of QC-1 to QC6: 1H and ^{13}C NMR spectra were recorded with a Bruker BioSpin GmbH spectrometer. High resolution mass spectra (HRMS) were recorded on a SCIEX TripleTOF 6600. The purities of the final compounds were confirmed to be higher than 95% by using analytical HPLC. Intermediates **2** and **QN-1** were synthesized according to our previous study.¹ The general method for synthesis of **QC-1–QC-6** is described below: the starting materials, including **QN-1** (1.0 mmol), N,N'-dimethyl-1,2-ethanediamine (or N,N'-dimethyl-1,3-propanediamine, or 2-methylaminoethanol, or 3-(methylamino)-1-propanol, or ethylene glycol, or 1,3-propanediol) (5.0 mmol) and K_2CO_3 (1.0 mmol), were dispersed and stirred in DMF under 100 °C overnight. After cooling, the mixture was poured into cold water, and the precipitate was filtered to get the final compound. If there was no precipitate, ethyl acetate was used to extract the crude product, and then it was purified using flash column chromatography to obtain the final product.

1,4-Dimethyl-7,8-bis(4-(4-methylpiperazin-1-yl)phenyl)-1,2,3,4-tetrahydropyrazino[2,3-g]quinoxaline (**QC-1**). Yellow solid. (72% yield). 1H NMR (600 MHz, $CDCl_3$) δ 7.42 (d, J = 8.8 Hz, 4H), 6.92 (s, 2H), 6.86 (d, J = 8.8 Hz, 4H), 3.54 – 3.44 (m, 4H), 3.30 – 3.19 (m, 8H), 3.06 (s, 6H), 2.65 – 2.56 (m, 8H), 2.37 (s, 6H). ^{13}C NMR (151 MHz, $CDCl_3$) δ 150.50, 148.38, 140.59, 138.18, 131.88, 130.63, 115.40, 103.87, 55.02,

49.05, 48.78, 46.13, 39.60.

4-Methyl-7,8-bis(4-(4-methylpiperazin-1-yl)phenyl)-3,4-dihydro-2*H*-[1,4]oxazino[2,3-*g*]quinoxaline (**QC-2**). Yellow solid (57% yield). ¹H NMR (600 MHz, CDCl₃) δ 7.44 (d, *J* = 1.9 Hz, 2H), 7.43 (d, *J* = 1.9 Hz, 2H), 7.37 (s, 1H), 7.09 (s, 1H), 6.87 (d, *J* = 3.0 Hz, 2H), 6.86 (d, *J* = 3.1 Hz, 2H), 4.44 – 4.38 (m, 2H), 3.50 – 3.42 (m, 2H), 3.30 – 3.19 (m, 8H), 3.08 (s, 3H), 2.62 – 2.56 (m, 8H), 2.37 (s, 6H). ¹³C NMR (151 MHz, CDCl₃) δ 150.86, 150.76, 150.70, 149.18, 147.81, 139.89, 139.15, 136.63, 131.27, 131.18, 130.66, 115.29, 111.41, 105.44, 64.82, 55.00, 48.65, 48.28, 46.14, 38.92.

7,8-Bis(4-(4-methylpiperazin-1-yl)phenyl)-2,3-dihydro-[1,4]dioxino[2,3-*g*]quinoxaline (**QC-3**). Pale yellow solid (45% yield). ¹H NMR (600 MHz, CDCl₃) δ 7.52 (s, 2H), 7.46 (d, *J* = 8.8 Hz, 4H), 6.87 (d, *J* = 8.8 Hz, 4H), 4.48 – 4.37 (m, 4H), 3.36 – 3.24 (m, 8H), 2.68 – 2.58 (m, 8H), 2.40 (s, 6H). ¹³C NMR (151 MHz, CDCl₃) δ 151.48, 151.02, 146.62, 137.69, 130.74, 130.66, 115.22, 113.10, 64.37, 54.91, 48.40, 46.04.

6,10-Dimethyl-2,3-bis(4-(4-methylpiperazin-1-yl)phenyl)-7,8,9,10-tetrahydro-6*H*-[1,4]diazepino[2,3-*g*]quinoxaline (**QC-4**). Yellow solid (66% yield). ¹H NMR (600 MHz, CDCl₃) δ 7.43 (d, *J* = 8.7 Hz, 4H), 7.27 (s, 2H), 6.87 (d, *J* = 8.8 Hz, 4H), 3.33 (t, *J* = 5.9 Hz, 4H), 3.29 – 3.21 (m, 8H), 3.03 (s, 6H), 2.64 – 2.55 (m, 8H), 2.37 (s, 6H), 1.95 – 1.88 (m, 2H). ¹³C NMR (151 MHz, CDCl₃) δ 150.77, 149.94, 147.40, 138.79, 131.33, 130.64, 115.32, 112.39, 54.99, 53.88, 48.66, 46.13, 42.53, 26.08.

10-Methyl-2,3-bis(4-(4-methylpiperazin-1-yl)phenyl)-7,8,9,10-tetrahydro-[1,4]oxazepino[2,3-*g*]quinoxaline (**QC-5**). Yellow solid (48% yield). ¹H NMR (600 MHz, CDCl₃) δ 7.53 (s, 1H), 7.44 (d, *J* = 8.5 Hz, 4H), 7.23 (s, 1H), 6.90 – 6.84 (m, 4H), 4.33 (t, *J* = 5.9 Hz, 2H), 3.51 – 3.44 (m, 2H), 3.32 – 3.23 (m, 8H), 3.08 (s, 3H), 2.67 – 2.55 (m, 8H), 2.38 (s, 6H), 2.19 – 2.10 (m, 2H). ¹³C NMR (151 MHz, CDCl₃) δ 153.70, 151.54, 150.95, 150.85, 150.01, 147.34, 139.58, 137.30, 131.06, 130.94, 130.69, 130.67, 117.49, 115.28, 115.25, 110.89, 70.21, 54.96, 52.94, 48.55, 46.11, 42.11, 29.08.

2,3-Bis(4-(4-methylpiperazin-1-yl)phenyl)-8,9-dihydro-7*H*-[1,4]dioxepino[2,3-*g*]quinoxaline (**QC-6**). Pale yellow solid (40% yield). ¹H NMR (600 MHz, CDCl₃) δ 7.64 (s, 2H), 7.46 (d, *J* = 8.8 Hz, 4H), 6.88 (d, *J* = 8.9 Hz, 4H), 4.40 (t, *J* = 5.7 Hz, 4H), 3.36 – 3.27 (m, 8H), 2.71 – 2.62 (m, 8H), 2.42 (s, 6H), 2.32 (dt, *J* = 11.5, 5.7 Hz, 2H). ¹³C NMR (151 MHz, CDCl₃) δ 154.03, 152.04, 151.04, 138.43, 130.77, 130.53, 117.99, 115.22, 70.56, 54.84, 48.26, 45.94, 29.71.

Table S1. DNA sequences used in the present study

Name	Sequence (from 5' to 3')	Structure
pu22	TGAGGGTGGGTAGGGTGGGTAA	parallel G4 ²
c-kit1	AGGGAGGGCGCTGGGAGGAGGG	parallel G4 ³
bcl-2	GGGCGGGCGCGGGAGGAAGGGGGCGGG	parallel G4 ⁴
kras	AGGGCGGTGTGGGAAGAGGGAAGAGGGGGAGG	parallel G4 ⁵
c-kit2	GGGCGGGCGCGAGGGAGGGG	parallel G4 ⁶
vegf	GGGGCGGGCCGGGGGCGGGG	parallel G4 ⁷
hras	TCGGTTGCGGGCGCAGGGCACGGGCG	antiparallel G4 ⁸
tel22	AGGGTTAGGGTTAGGGTTAGGG	mixed G4 ⁹
hairpin	CGCGCGCTTTTCGCGCGCG	duplex DNA
ds26	CAATCGGATCGAATTCGATCCGATTG	duplex DNA
tel22-ap1	(2- <i>Ap</i>)GGGTTAGGGTTAGGGTTAGGG	mixed G4
tel22-ap7	AGGGTT(2- <i>Ap</i>)GGGTTAGGGTTAGGG	mixed G4
tel22-ap13	AGGGTTAGGGTT(2- <i>Ap</i>)GGGTTAGGG	mixed G4
tel22-ap19	AGGGTTAGGGTTAGGGTT(2- <i>Ap</i>)GGG	mixed G4

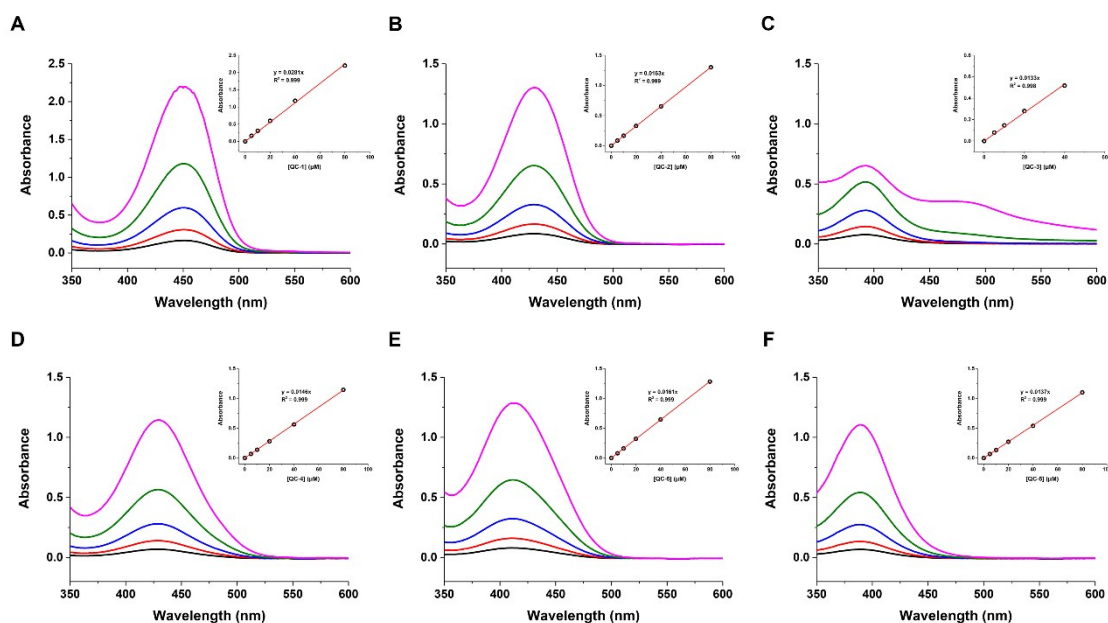


Figure S1. Concentration-dependent absorption spectra of the quinoxaline derivatives (**QC-1–QC-6**) in Tris-HCl buffer. A linear correlation was found between the absorbance intensities and the compound concentrations (0–40 μM), indicating that the compounds little propensity to aggregate in Tris-HCl buffer. **QC-3** tended to aggregate in the buffer when its concentration reached over 40 μM .

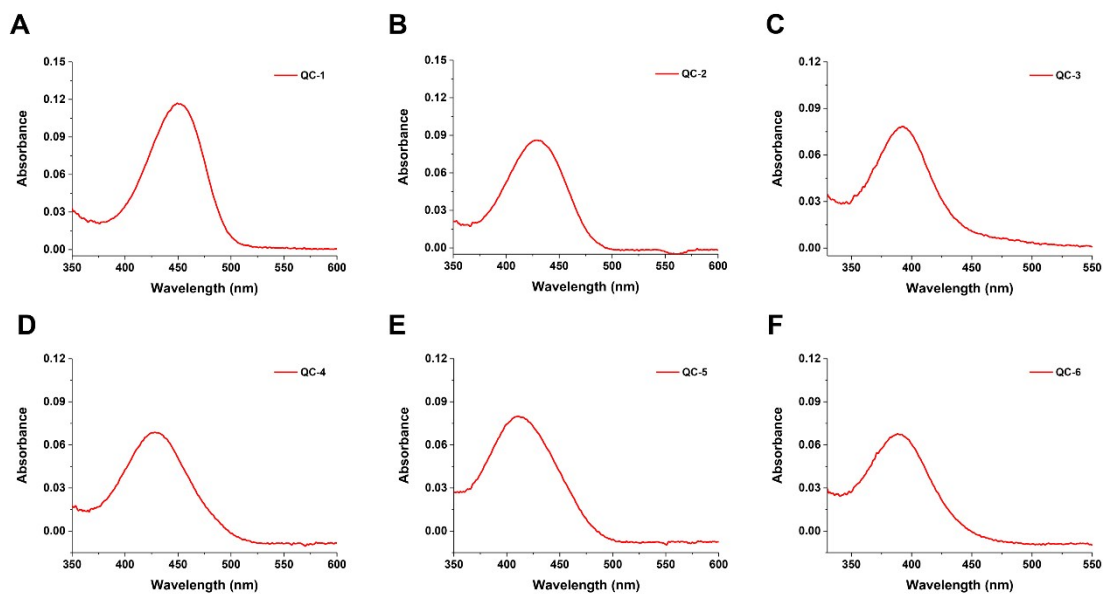


Figure S2. Absorption spectra of the quinoxaline derivatives (**QC-1–QC-6**) at 5 μ M in Tris-HCl buffer

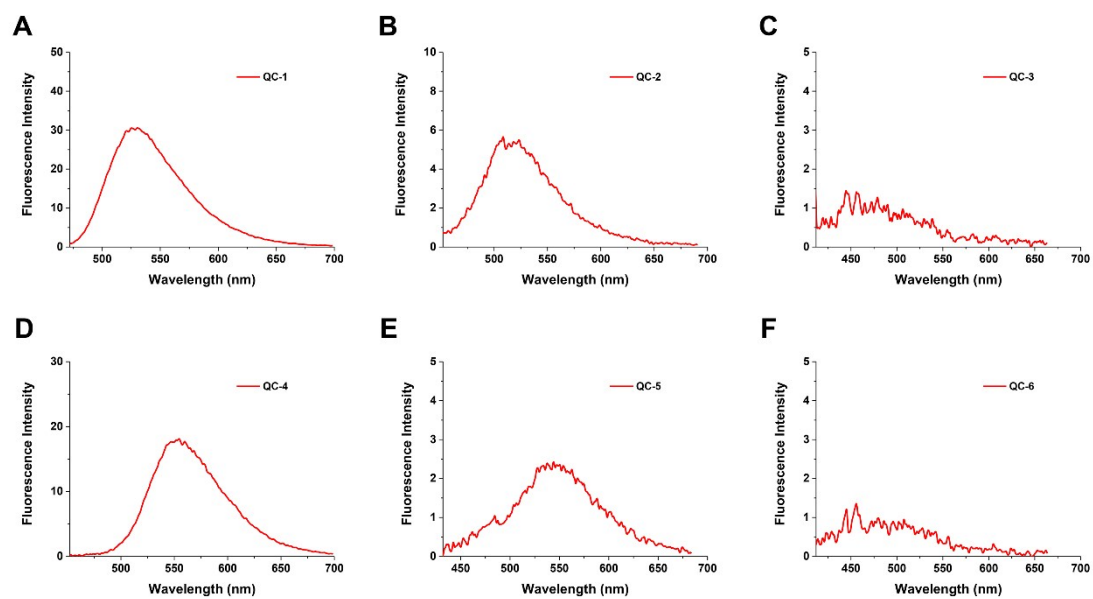


Figure S3. Fluorescence spectra of the quinoxaline derivatives (**QC-1–QC-6**) at 1 μ M in Tris-HCl buffer

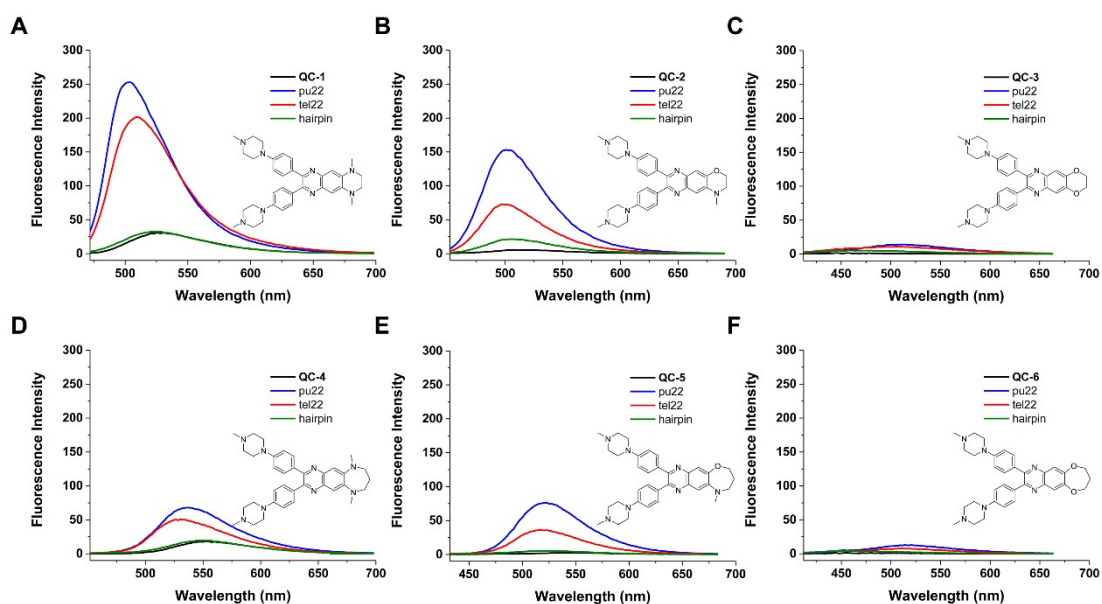


Figure S4. Fluorescence spectra of the quinoxaline derivatives (**QC-1–QC-6**) upon interaction with parallel G4 pu22, nonparallel G4 tel22 and duplex DNA hairpin in Tris-HCl buffer.

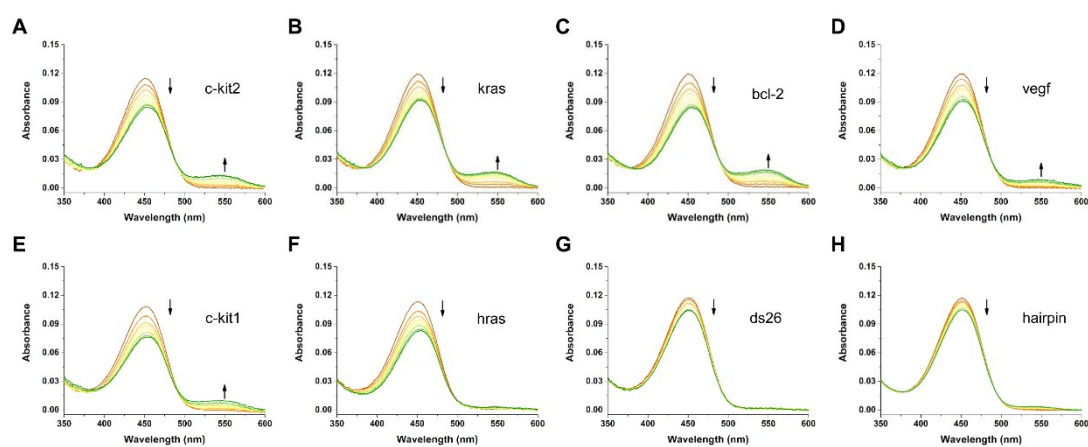


Figure S5. Absorption spectra of **QC-1** (5 μM) upon gradual addition of types of nucleic acids (0–5 μM): (A) parallel G4 c-kit2, (B) parallel G4 kras, (C) parallel G4 bcl-2, (D) parallel G4 vegf, (E) parallel G4 c-kit1, (F) nonparallel G4 hras, (G) duplex DNA ds26 and (H) duplex DNA hairpin in Tris-HCl buffer. Arrows indicate the absorbance changes.

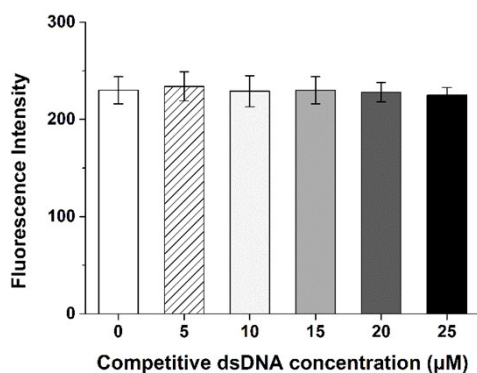


Figure S6. Fluorescence intensities of **QC-1**-pu22 complex with gradual addition of competitive duplex DNA in Tris-HCl buffer, $\lambda_{\text{ex}} = 450$ nm. The data indicated that in the presence of excess duplex DNA competitor, the enhanced fluorescence of **QC-1** with pu22 was only slightly affected, suggesting the binding selectivity of **QC-1** to G4.

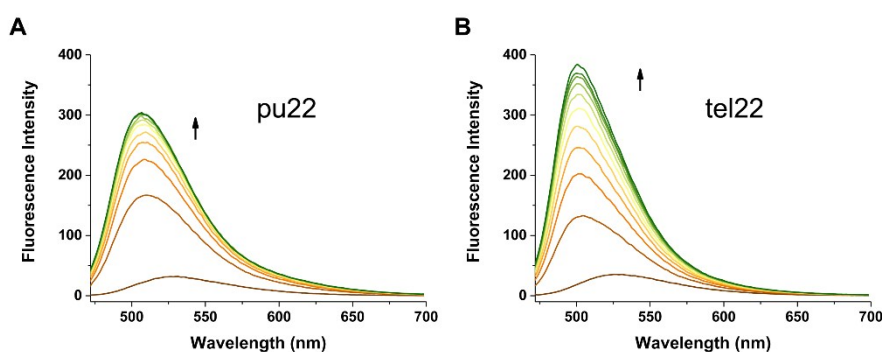


Figure S7. Fluorescence spectra of 1 μM **QC-1** with the stepwise addition of G4 samples in Tris-HCl buffer, $\lambda_{\text{ex}} = 450$ nm: (A) parallel G4 pu22 and (B) nonparallel G4 tel22 (arrow: 0–10 mol equiv.).

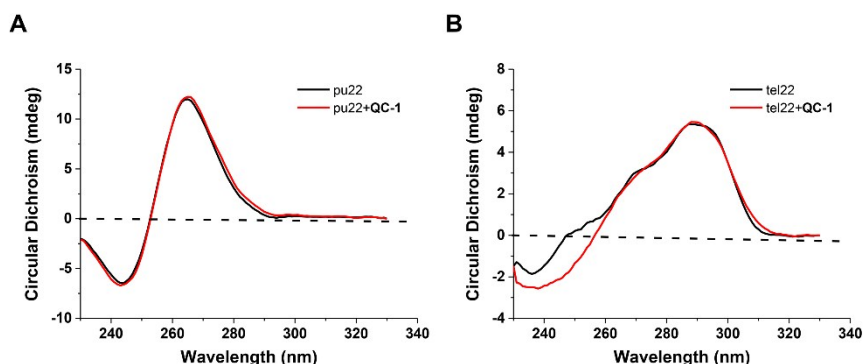


Figure S8. The CD spectra of (A) parallel G4 pu22 and (B) nonparallel G4 tel22 with or without **QC-1** in Tris-HCl buffer. The DNA concentrations were set as 2 μM , and the concentration of **QC-1** was 6 μM .

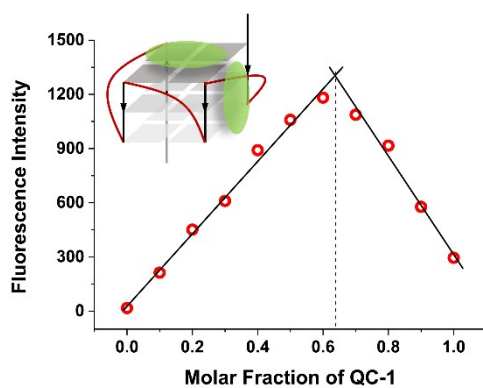


Figure S9. Job plot analysis for the binding stoichiometry of **QC-1** to parallel G4 pu22. The turning point is near 0.66, showing a 2:1 stoichiometry.

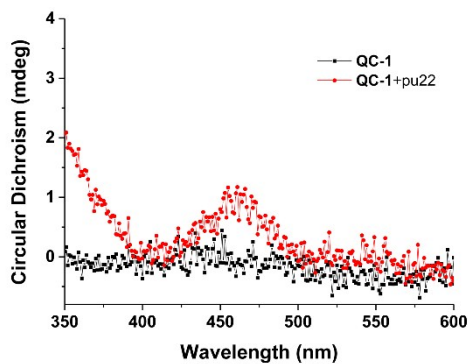


Figure S10. CD spectra of **QC-1** (30 μM) with or without parallel G4 pu22 (20 μM) in Tris-HCl buffer. It shows a small induced CD signal for **QC-1**.

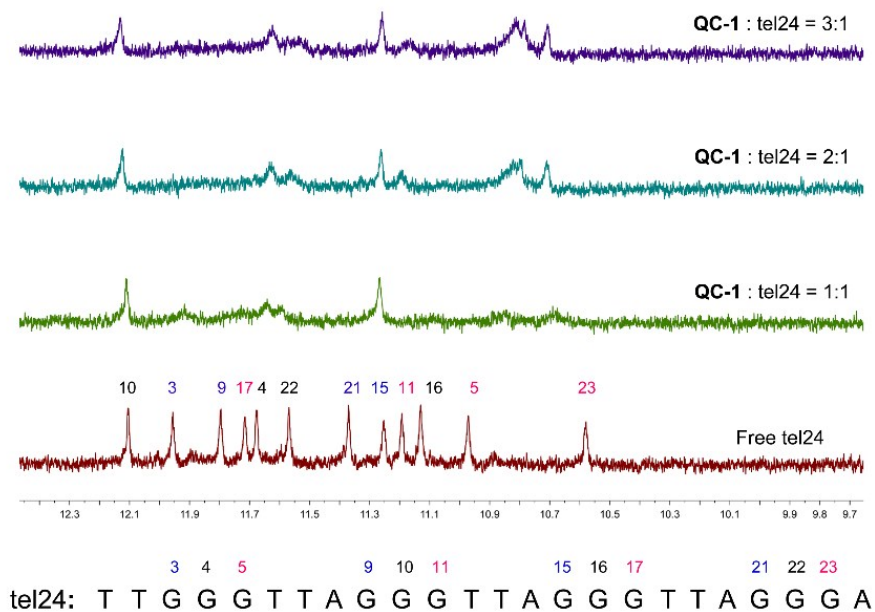


Figure S11. Imino proton regions of the $^1\text{H-NMR}$ spectra of nonparallel (3+1) G4 tel24 either alone or with **QC-1**. Guanines from the 5'-end G-tetrad are colored in blue, the middle G-tetrad in black, and the 3'-end G-tetrad in red.

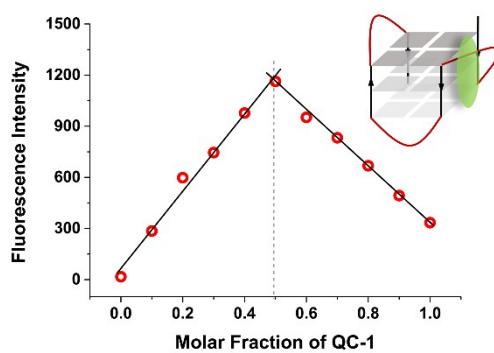


Figure S12. Job plot analysis for the binding stoichiometry of **QC-1** to nonparallel G4 tel22. The turning point is near 0.5, showing a 1:1 stoichiometry.

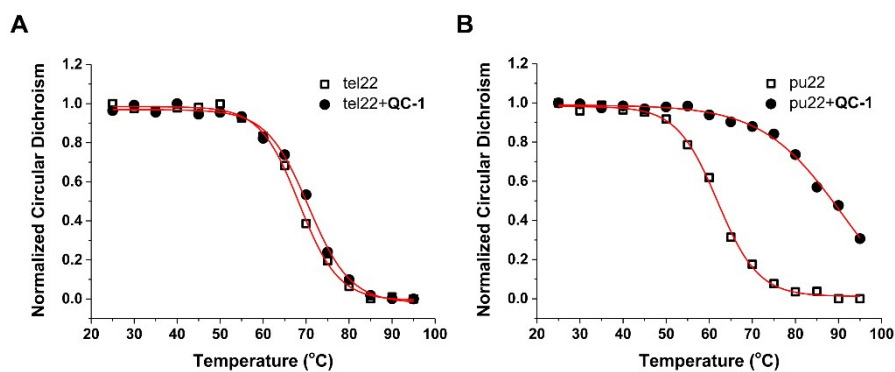


Figure S13. CD melting curves for G4s in the absence and presence of 3 equiv. of **QC-1**: (A) nonparallel G4 tel22 and (B) parallel G4 pu22.

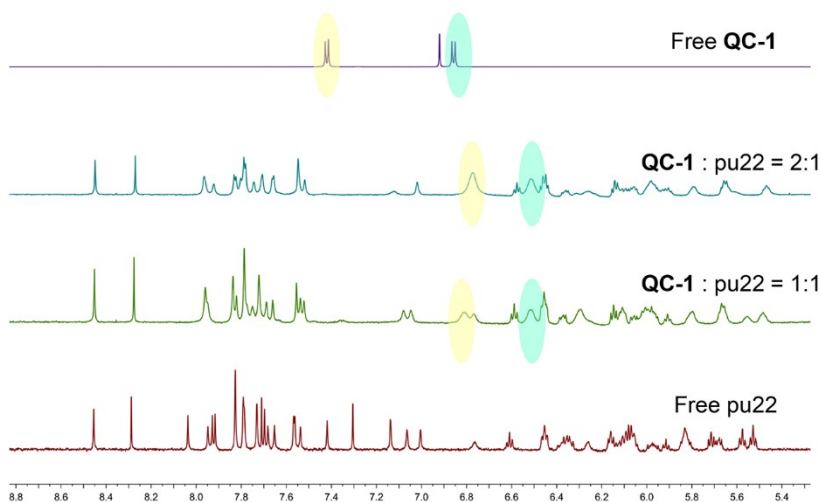


Figure S14. Aromatic regions of the ¹H-NMR spectra of **QC-1** without and with G4. The proton signals underwent significant chemical shift perturbations.

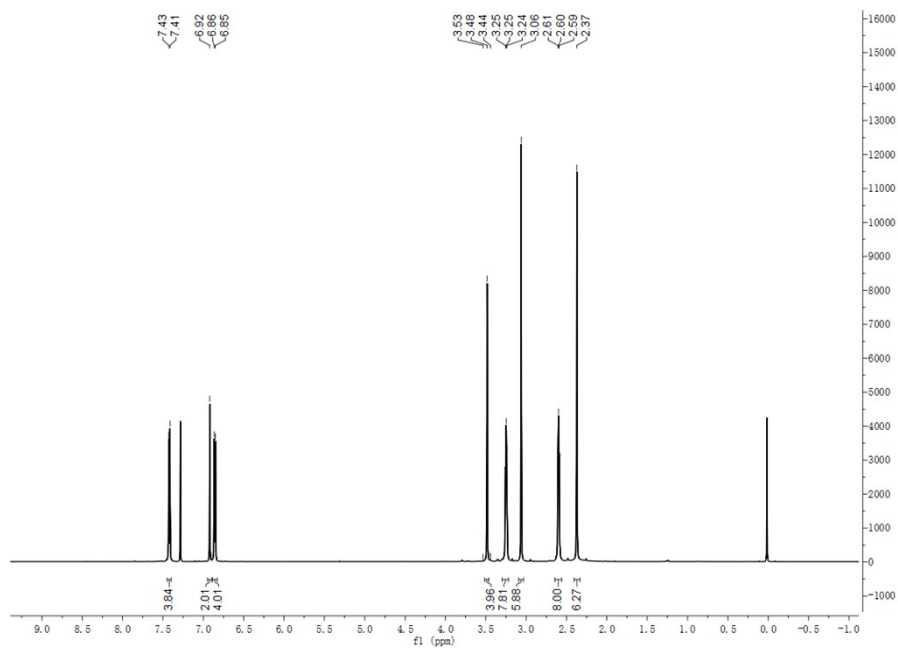


Figure S15. ¹H NMR spectrum of QC-1

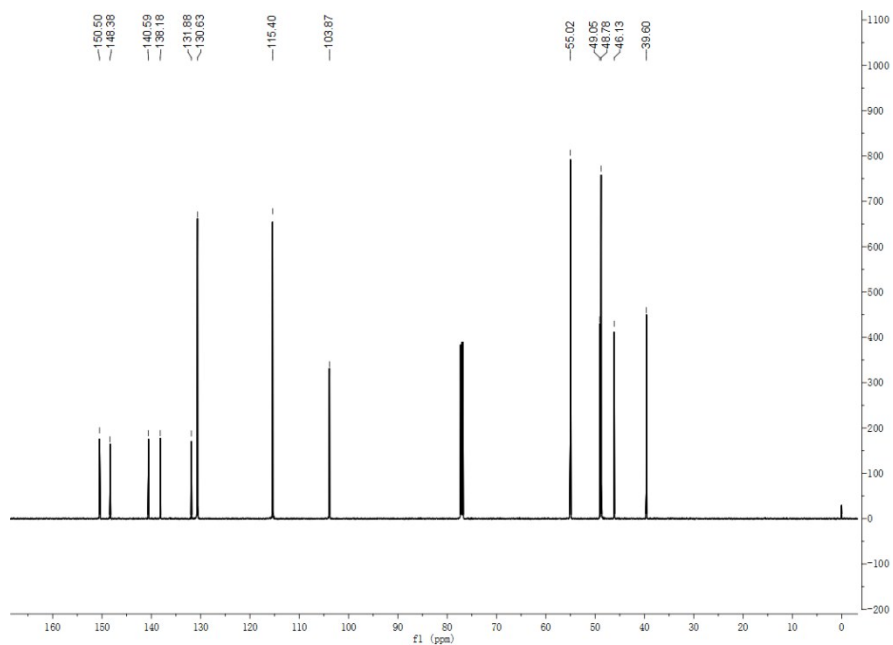


Figure S16. ¹³C NMR spectrum of QC-1

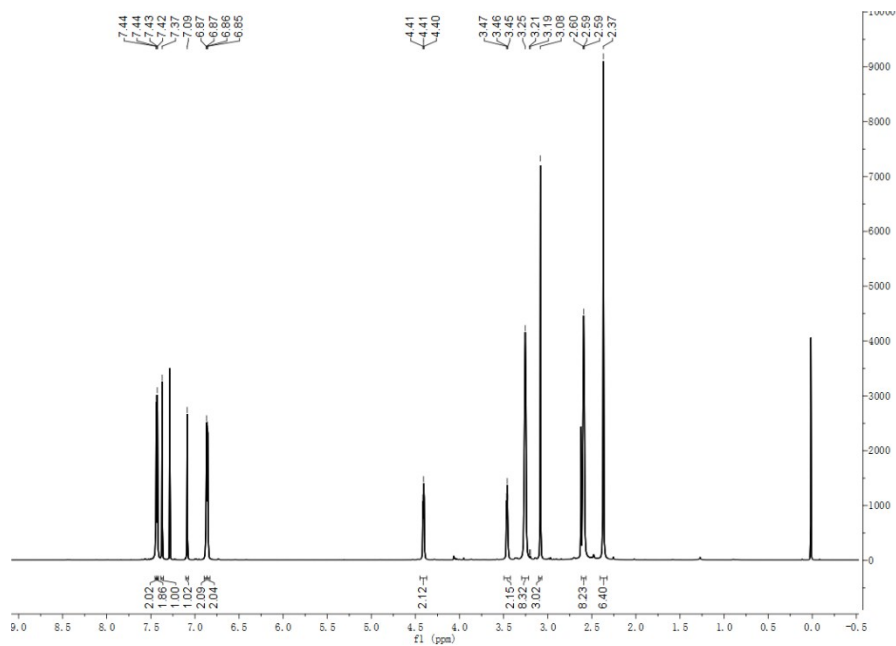


Figure S17. ¹H NMR spectrum of QC-2

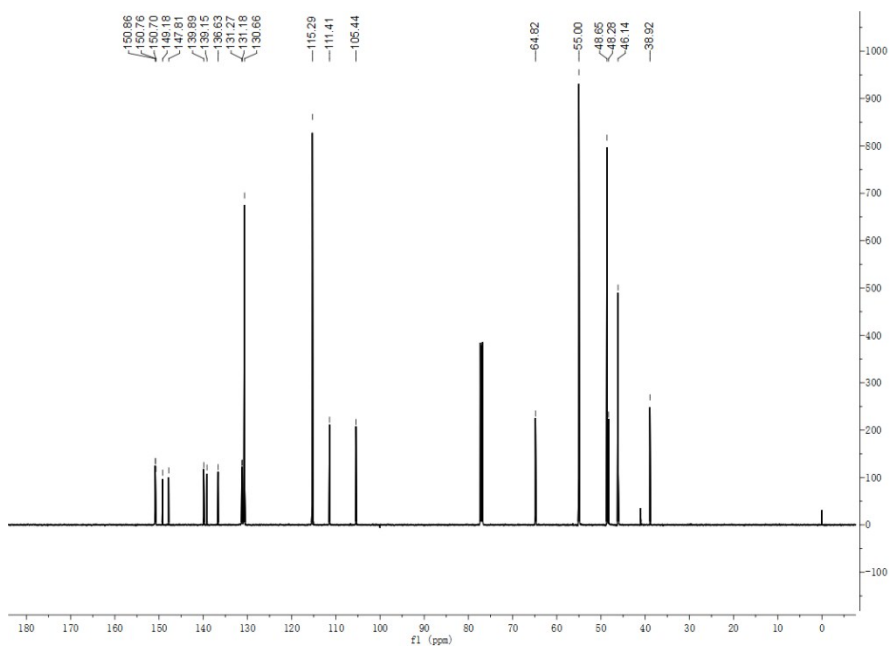


Figure S18. ¹³C NMR spectrum of QC-2

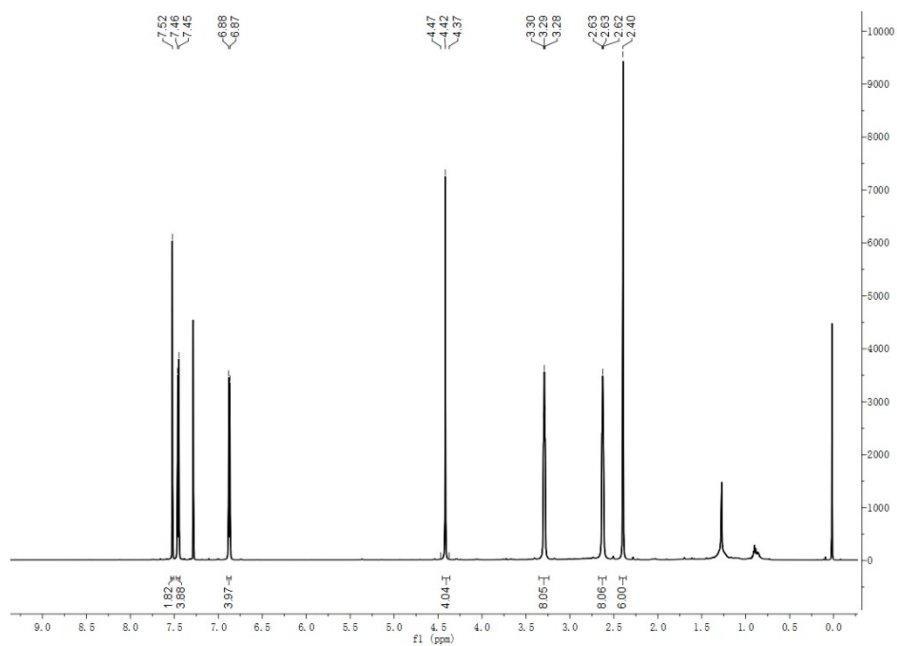


Figure S19. ¹H NMR spectrum of QC-3

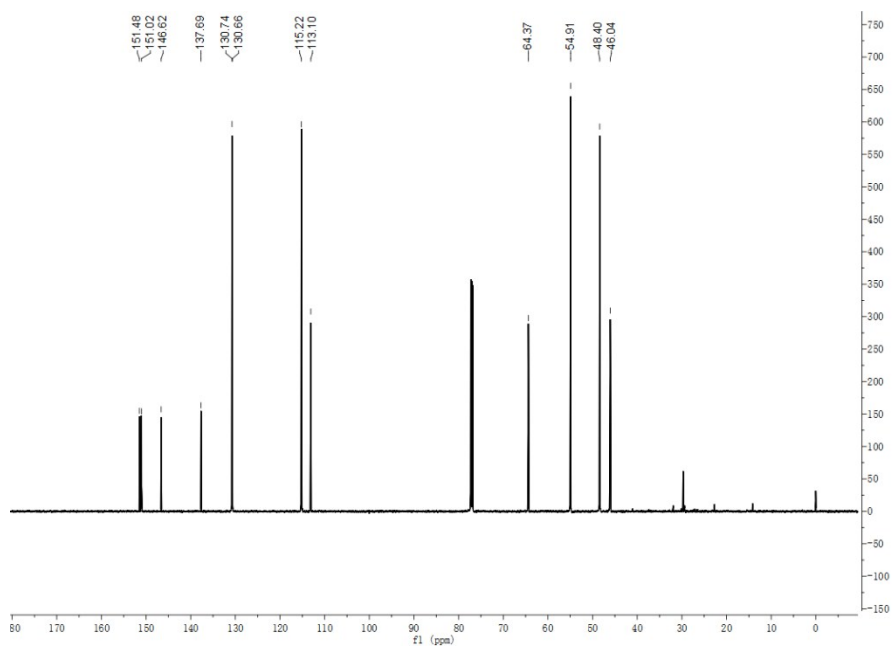


Figure S20. ¹³C NMR spectrum of QC-3

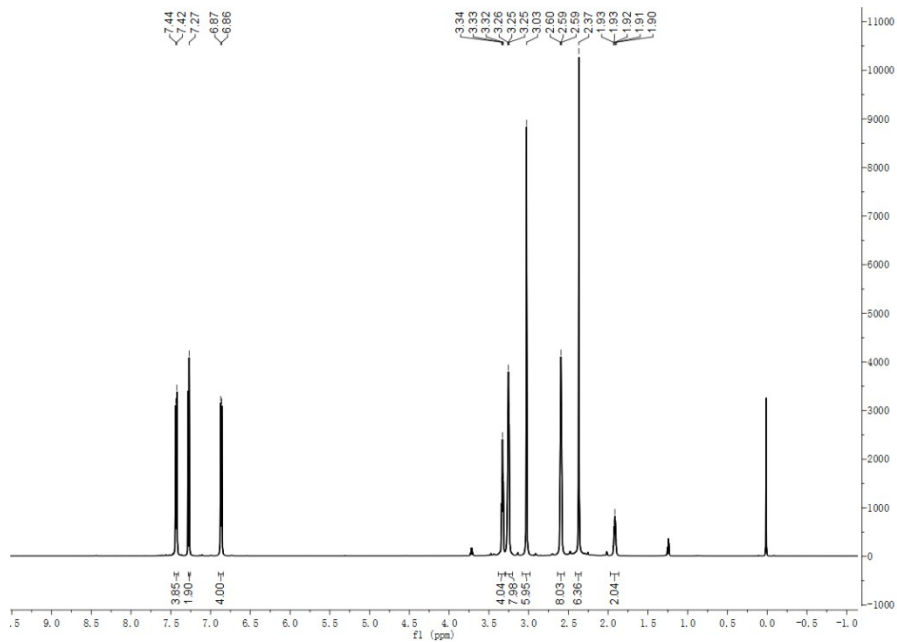


Figure S21. ¹H NMR spectrum of QC-4

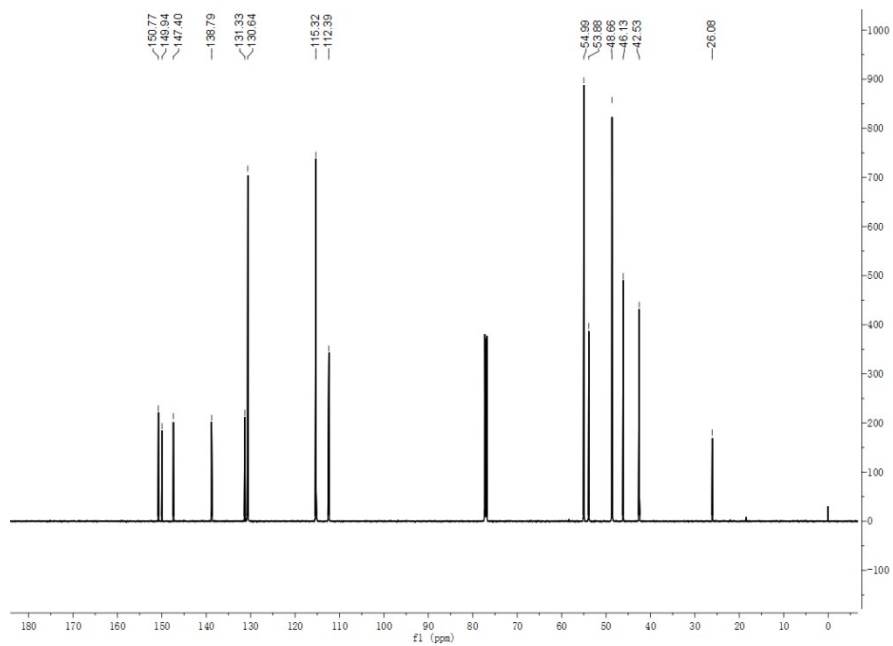


Figure S22. ¹³C NMR spectrum of QC-4

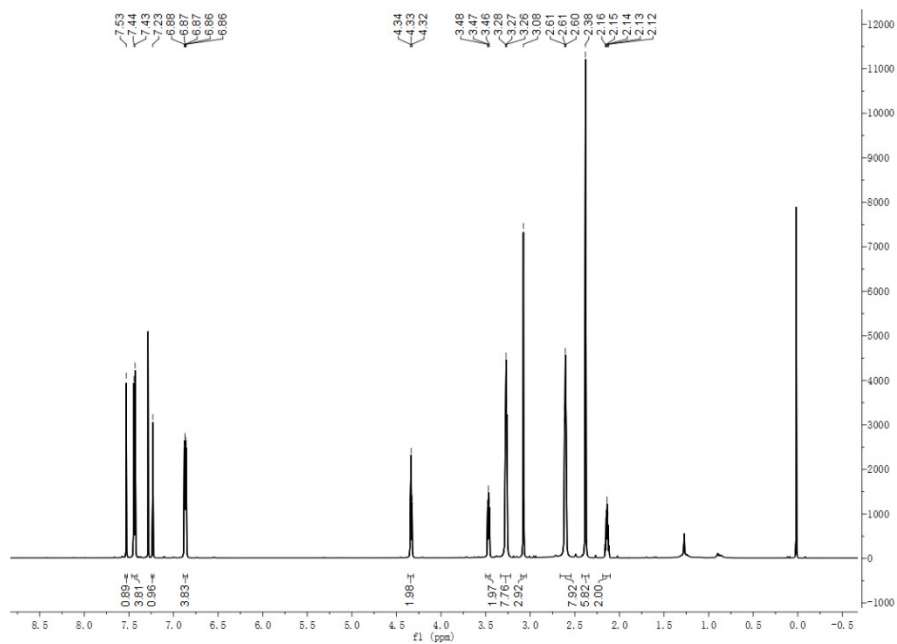


Figure S23. ¹H NMR spectrum of QC-5

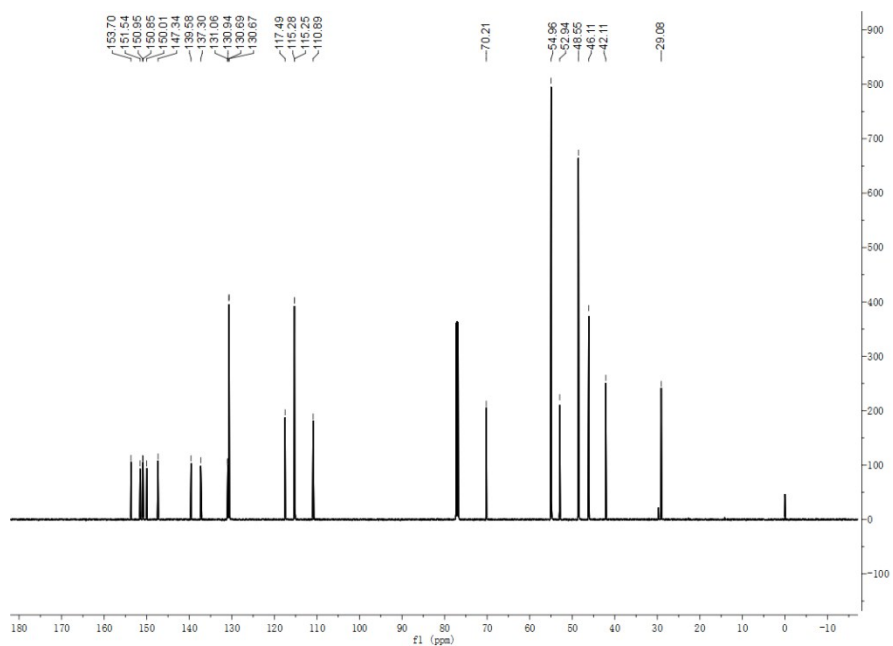


Figure S24. ¹³C NMR spectrum of QC-5

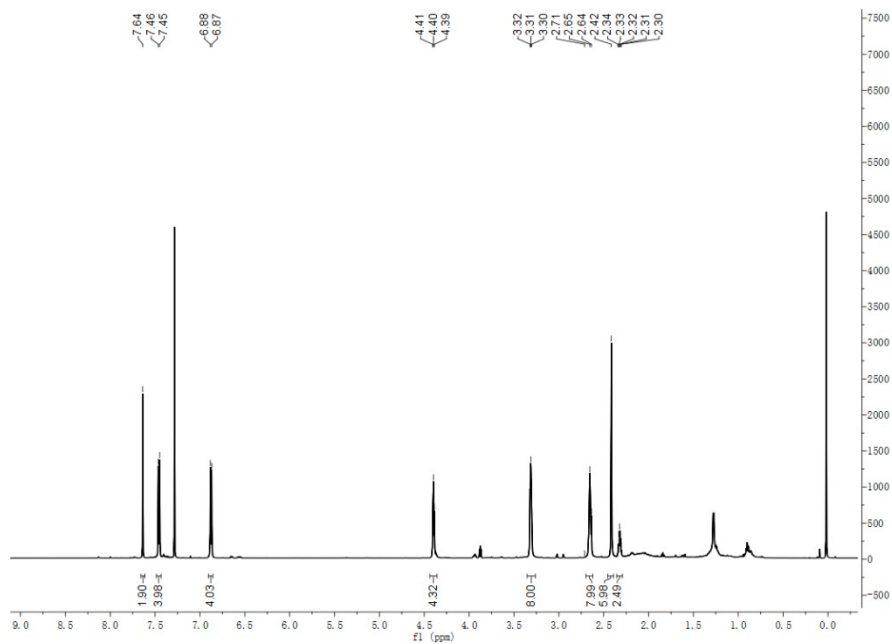


Figure S25. ¹H NMR spectrum of QC-6

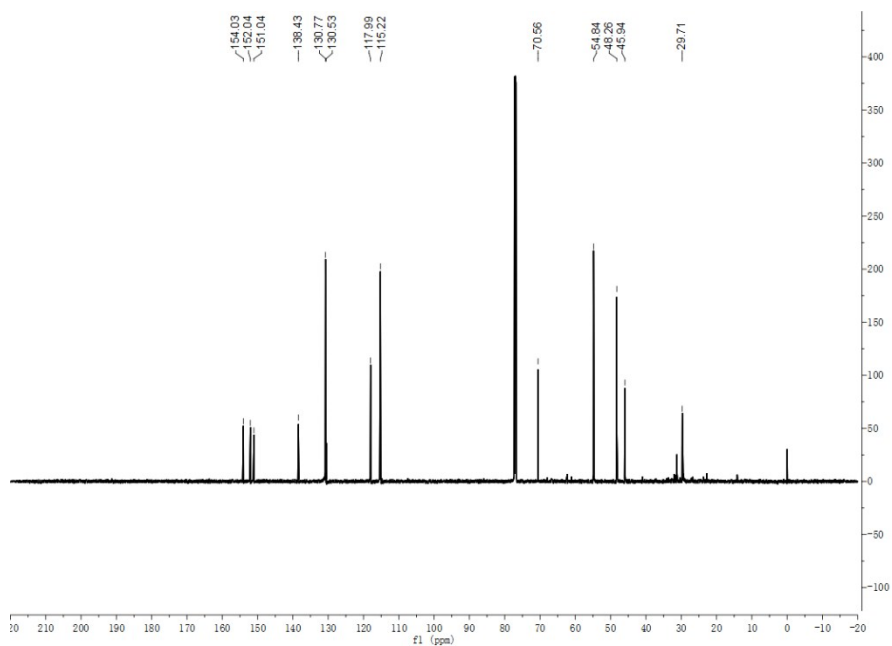


Figure S26. ¹³C NMR spectrum of QC-6

References

1. M.-H. Hu, T.-Y. Wu, Q. Huang and G. Jin, *Nucleic Acids Res.*, 2019, **47**, 10529-10542.
2. A. T. Phan, Y. S. Modi and D. J. Patel, *J. Am. Chem. Soc.*, 2004, **126**, 8710-8716.
3. S. Rankin, A. P. Reszka, J. Huppert, M. Zloh, G. N. Parkinson, A. K. Todd, S. Ladame, S. Balasubramanian and S. Neidle, *J. Am. Chem. Soc.*, 2005, **127**, 10584-10589.
4. J. Dai, T. S. Dexheimer, D. Chen, M. Carver, A. Ambrus, R. A. Jones and D. Yang, *J. Am. Chem. Soc.*, 2006, **128**, 1096-1098.
5. S. Cogoi and L. E. Xodo, *Nucleic Acids Res.*, 2006, **34**, 2536-2549.
6. S.-T. D. Hsu, P. Varnai, A. Bugaut, A. P. Reszka, S. Neidle and S. Balasubramanian, *J. Am. Chem. Soc.*, 2009, **131**, 13399-13409.
7. D. Sun, K. Guo and Y.-J. Shin, *Nucleic Acids Res.*, 2011, **39**, 1256-1265.
8. A. Membrino, S. Cogoi, E. B. Pedersen and L. E. Xodo, *PLoS ONE*, 2011, **6**, e24421.
9. A. T. Phan, V. Kuryavyi, K. N. Luu and D. J. Patel, *Nucleic Acids Res.*, 2007, **35**, 6517-6525.